

Physics of Lumen growth

Sabyasachi Dasgupta^{a,b}, Kapish Gupta^a, Yue Zhang^a, Virgile Viasnoff^{a,c,d,1}, and Jacques Prost^{a,b}

^aMechanobiology Institute, National University of Singapore, Singapore 117411, Singapore; ^bLaboratoire Physico Chimie Curie, Institut Curie, PSL Research University, CNRS UMR168, 75005 Paris, France; ^cCNRS UMI3639, Singapore 117411, Singapore; ^dDepartment of Biological Sciences, National University of Singapore, Singapore 117411, Singapore

This manuscript was compiled on April 3, 2018

We model the dynamics of formation of intercellular secretory lumens. Using conservation laws, we quantitatively study the balance between paracellular leaks and the build-up of osmotic pressure in the lumen. Our model predicts a critical pumping threshold to expand stable lumens. Consistently with experimental observations in bile canaliculi, the model also describes a transition between a monotonous and oscillatory regime during luminogenesis as a function of ion and water transport parameters. We finally discuss the possible importance of regulation of paracellular leaks in intercellular tubulogenesis.

osmoregulation | membrane pumps | lumens | tissue mechanics |

Epithelial lumens are ubiquitous in organs. They originate from cavities or tubes surrounded by one (seamless lumen) or multiple cells (1). Ions and other bioactive molecules are secreted into the cavities and, if the lumen is open, flow with the physiological medium. The creation of the lumens originates from several classes of morphogenetic events (1). In the case of closed lumens (such as acini, blastocytes, canaliculi), ion secretion into the forming cavity creates an osmotic pressure. This results in the passive transport of water into the lumen (most often mediated by aquaporins), which constitutes a major driving component for lumen expansion. This osmotic pressure hypothesis was experimentally proposed in the 1960s (2–4). The expansion is mechanically restrained by periluminal tension. In the case of multicellular lumens (eg: cysts (5–7)), tension results from the contraction of the cells surrounding the lumen. In the case of the intercellular domain, the tension arises from the cortical actin layer surrounding the cavity (8).

Fig. 1a illustrates a lumen separating adjacent membranes between two primary rat hepatocytes (liver cells). The contact area between both cells presents an intercellular cleft of around 30–50 nm (9) that accommodates transcellular proteins, adhesion proteins and peptidoglycans. The development of the lumen occurs within 5 to 6 hours. *In vivo*, closed lumens eventually merge into a network of tubules called canaliculi (2 μm diameter and 500 μm long). We recently showed that the shape of these lumen is controlled by the balance of osmotic pressure and anisotropic cortical tension (10). Hepatocyte doublets can be used as meaningful simplified surrogates to study lumen formation (8, 11, 12). In this instance functional canaliculi grow as spherical caps spanning part of the intercellular space. The simple geometry of the system constitutes an appealing case for quantitative studies.

However, this process is rather generic for many kinds of lumen such as Ciona Notochord lumen (1, 13, 14) or kidney lumens (15). Fig. 1b–c also shows that the steady shape of the lumen depends on the secretory activity, which is boosted by the addition of Ursodeoxycholic acid (UDCA). The growth of the lumen can either be monotonous (Fig. 1c) or pulsatile

(Fig. 1d) depending on the periluminal tension and secretory activity. A steady secretion in a closed lumen implies the concomitant existence of leakage. Its nature is likely paracellular (through the nanometer cleft between cells). In the case of multicellular lumen, a few models and experimental studies have considered the role of leaks (originating either from the rupture of cell-cell contacts (7) or permeation across the endothelial layer (16)) during the growth of the lumen. For intercellular lumens, however, the morphogenetic consequences of the leak modulation by the paracellular cleft property have hardly been investigated, either experimentally or theoretically.

Here, we provide a theoretical quantitative study on the balance between secretory activity, leak and mechanics that determines canaliculi nucleation and growth. Our minimalistic description of lumen expansion identifies the physiologically relevant range of parameters required to establish a stable intracellular cavity and dictate its dynamical properties.

Modeling Assumption

We consider the lumen as two symmetrical contractile spherical caps (Fig. 2) with a radius of curvature R and a contact angle θ at the lumen edge. The lumen elongates parallel to the cell-cell contact over a distance r_l and its apex height is h . The remaining paracellular adhesive cleft has a thickness e . As the lumen develops, the dimension of the spherical caps vary but the cell contact remains fixed with a total size L . We established the expressions of the conservation laws in the lumen and in the cleft accounting for this geometry. All results are in the scaled units of the model (See SI appendix, Table

Significance Statement

The development of intercellular cavities (lumens) is a ubiquitous mechanism to form complex tissue structures in organisms. The generation of Ciona notochord, the formation of Zebrafish vasculature, or of bile canaliculi between hepatic cells constitute a few examples. Lumen growth is governed by water intake that usually results from the creation of salt concentration difference (osmotic gradients) between the inside and the outside of the lumen. During morphogenesis or in diseases, lumens can also leak due to improper maturation of the cell junctions that seal them. In this paper, we theoretically describe different conditions and dynamical regimes of lumen growth based on the balance of osmotic pressure, fluid intake and paracellular leak.

S.D performed the numerical and symbolic calculations. K.G and YZ measured the lumen dynamics changes. V.V and J.P proposed the model. J.P derived the solutions. V.V designed the figures. J.P and V.V jointly wrote the manuscript.

The Authors declare no conflict of interest.

¹To whom correspondence should be addressed. E-mail: virgile.viasnoff@espci.fr, jacques.prost@curie.fr

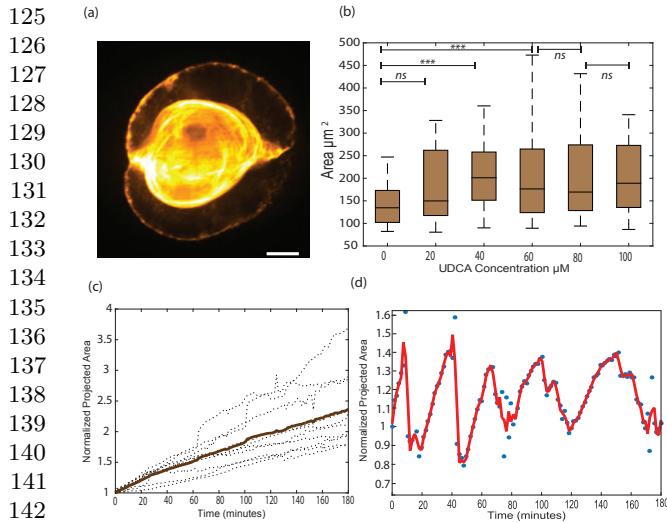


Fig. 1. a: Structured illumination image of a typical bile canaliculi creating a lumen between two hepatocytes (scale bar $2 \mu\text{m}$). b: Increase of projected area of canaliculi at steady state upon continuous bile secretion stimulation by different dose of UDCA (Ursodeoxycholic acid) ($n=20$ for each dose). c: Linear growth of the canaliculi (dotted line: individual cell, bold line: average) under reduced contractility condition ($1 \mu\text{M}$ blebbistatin) d: Sustained Oscillatory dynamics under native contractility conditions. Bile canaliculi projected area are normalized by their size at $t=0$

S1) as well as in "international units" based on the estimations derived in SI Appendix (2).

We study the lumen growth dynamics resulting from the balance between *i* the active and passive ion transport across membranes both in the lumen and in the cleft; *ii* the passive transport of water along transmembrane osmotic and hydrostatic gradients; *iii* the paracellular leakage originating from osmotic gradients and hydrostatic gradients along the cleft; *iv* the mechanical balance controlled by actomyosin contractility. For the sake of simplicity, we considered only one type of anion/cation pair with identical transport properties. These simplified assumptions lead us to consider only ion, water and momentum conservations (i.e, force balance).

Mechanical balance. In the **lumen** the hydrostatic pressure δP is uniform at the time scales considered here. Laplace's law must be satisfied everywhere across the lumen surface. The force balance in the lumen then reads:

$$\delta P = \frac{2\sigma}{R}. \quad [1]$$

Where σ is the cortical tension resulting from the sum of the plasma membrane tension and the active tension of the actin cortex. In general, the effective tension could be inhomogeneous and anisotropic (17). For example, in the late stages of Ciona Notochord lumen growth, or during the tubulation of canaliculi, the departure from a hemispherical shape results in inhomogeneous curvature radii, which is indicative of heterogeneous tension distributions (1, 13, 14). However, here we only consider an homogeneous cortical tension, consistent with the assumption that the lumen shape is a spherical cap.

In the **cleft**, Laplace's law must be modified to account for membrane adhesion (mediated by Cadherin for example (18))

$$\delta P = k(e - e_0) - \sigma_c \nabla^2 e, \quad [2]$$

e_0 is the cleft thickness in the absence of a difference in hydrostatic pressure. This is mainly controlled by the cadherin

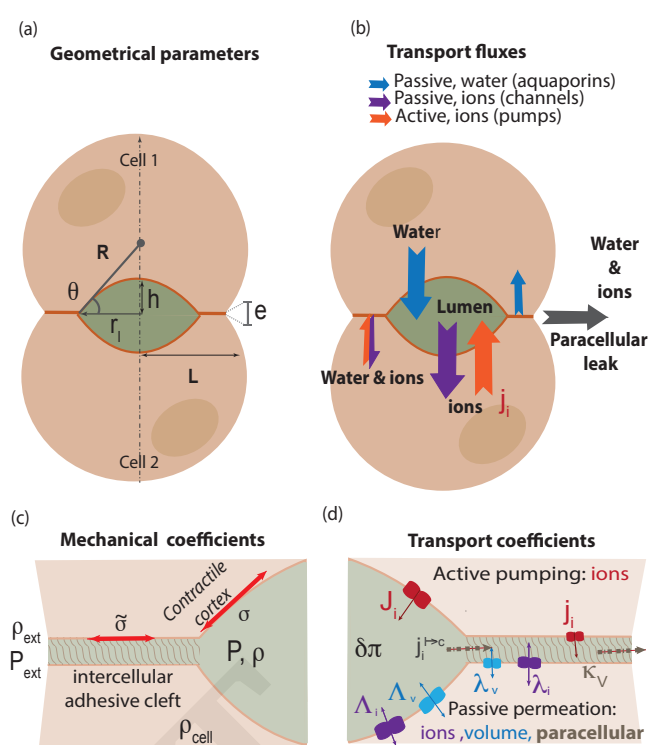


Fig. 2. Schematic for lumen at the interface of two adjacent cells. A: Definition of the geometrical parameters of the problem. b: Definition of the active and passive fluxes of Ion and water fluxes across and along the paracellular cleft. C: definition of the mechanical parameters of the problem. Close up on the intercellular cleft region containing adhesive molecules, peptidoglycans and other transmembrane proteins d: Definitions of the transport parameters.

surface density, as well as the repulsive interaction between the membranes. The parameter k is an effective elastic modulus that accounts for any deviation of the cleft from e_0 , accounting for tension in the cadherins and deformation of the membranes. In SI Appendix (2) we estimate that a few tens of nanometer away from the interfacial region, between the lumen and the cleft, equation 2 results in a homogeneous cleft thickness that hardly deviates from e_0 . In the rest of the paper equation 2 will be replaced by a homogeneous cleft thickness e . In the first order approximation $\delta P = k(e - e_0)$.

The force balance at the intersection of the lumen with the cleft is the generalized Young-Dupr  equation

$$\sigma \cos \theta = \sigma - E = \tilde{\sigma}, \quad [3]$$

where θ is the contact angle (see Fig. 2), E is the adhesion energy per unit area, $\tilde{\sigma}$ corresponds to the "apparent tension" corrected for the adhesion energy. The force balance is thus given by the set of equations 1 and 3.

Ion conservation. In the **lumen**, ion transport occurs by transmembrane fluxes, as well as by leakage at the lumen edges. The number of ions flowing through the membrane per unit of time and unit of area, has two distinct origins. First, an "active" flux per unit area J_i is generated by pumps and transporters. We assume that the flux has a constant value due to a constant surface density of the relevant pumps. Ions are also passively transported across trans-membrane

249 channels. In this case, the flux is proportional to the chemi- 311
 250 cal potential difference. It reads $\Lambda_i k_B T \ln \frac{\rho_{cell}}{\rho}$ where ρ_{cell}, ρ 312
 251 are the ion density in the cell cytoplasm and in the lumen 313
 252 respectively. The transport coefficient Λ_i is set by the surface 314
 253 density of the relevant channels. By convention all fluxes are 315
 254 positive when ions are secreted into the lumen. 316
 255 The conservation of the total number of ions, N , in the lumen 317
 256 then reads 318

$$257 \frac{dN}{dt} = \underbrace{[4\pi R^2(1 - \cos \theta)] (\Lambda_i k_B T \ln \frac{\rho_{cell}}{\rho} + J_i)}_{\text{surface term}} - \underbrace{[2\pi r_l] j_i^{l \rightarrow c}}_{\text{edge term}}, \quad [4]$$

262 The edge term $j_i^{l \rightarrow c}$ corresponds to the ion flux from the lumen 319
 263 into the cleft. It is determined self consistently by continuity 320
 264 conditions with the expression of the ion flux inside the cleft. 321

265 In the **cleft**, the ion density equilibrates within less than a 322
 266 few microseconds across the cleft thickness e (on the order of 323
 267 a few tens of nanometers). Hence, only the ion flux compo- 324
 268 nent along the cleft should be considered. The difference in 325
 269 ion concentration in the lumen, as compared to the external 326
 270 medium, generates a diffusive flux $-eD\nabla\rho$ along the ion con- 327
 271 centration gradient. D is the diffusion coefficient of ions. We 328
 272 neglect all convective contribution to the flux based on the 329
 273 small dimensions of the cleft. Under these assumptions, and 330
 274 after integration over the constant thickness e , the local and 331
 275 time dependent conservation of ions inside the cleft reads 332

$$276 \underbrace{\frac{\partial(\rho e)}{\partial t}}_{\text{negligible}} - D\Delta(e\rho) = 2(\lambda_i k_B T \ln \frac{\rho_{cell}}{\rho} + j_i). \quad [5]$$

281 where λ_i is the passive transport coefficient for ions through 333
 282 the membrane into the cleft. j_i is the active pumping of ions. 334
 283 The factor of 2 in the source term accounts for the presence of 335
 284 membranes from both cells. In SI Appendix (2) we show that 336
 285 that the term $\frac{\partial(\rho e)}{\partial t}$ is negligible on the time scale of lumen 337
 286 growth and will further be neglected. $j_i^{l \rightarrow c}$ in Eq. (4) is 338
 287 the solution of equation 5 at $r = r_l$. 339

290 **Volume conservation.** In view of the absence of an active bio- 340
 291 logical transport of water, the change in volume results solely 341
 292 from passive fluxes. Due to water incompressibility, the rate of 342
 293 volume change is proportional to the flux of water. The passive 343
 294 contribution from transmembrane water permeation is pro- 344
 295 portional to the water chemical potential difference and reads 345
 296 $-\Lambda_V(\delta P - \delta\pi)$. δP (resp $\delta\pi$) is the difference in hydrostatic 346
 297 (resp osmotic) pressure between the lumen and the cytosol. 347
 298 The surface density of aquaporins determines the transport 348
 299 coefficient Λ_V . The osmotic pressure difference is related to 349
 300 the ion density difference by $\delta\pi = 2k_B T(\rho - \rho_{cell})$. The factor 350
 301 2 in this expression reflects the equivalent treatment of anions 351
 302 and cations. The conservation of volume in the **lumen** then 352
 303 reads 353

$$304 \frac{dV}{dt} = \underbrace{-\Lambda_V [4\pi R^2(1 - \cos \theta)] (\delta P - \delta\pi)}_{\text{surface term}} - \underbrace{[2\pi l] j_V^{l \rightarrow c}}_{\text{edge term}}, \quad [6]$$

308 The volume leak $j_V^{l \rightarrow c}$ from the lumen into the cleft is deter- 354
 309 mined by continuity of the expression of the volume flux in 355
 310 the cleft at the lumen/cleft interface. 356

311 In the **cleft**, the rapid equilibration of the hydrostatic 312
 312 pressure across the cleft justifies the lubrication approximation 313
 313 to estimate the hydrodynamic contribution of volume change 314
 314 by $-\kappa_V \nabla P$. Note that, due to protein crowding at the 315
 315 paracellular cleft, κ_V is necessarily smaller than the Poiseuille 316
 316 limit $\frac{e^3}{12\eta}$ where η is the viscosity of the intercellular fluid. The 317
 317 local volume conservation in the cleft then reads 318

$$319 \underbrace{\frac{\partial e}{\partial t}}_{\text{negligible}} - \nabla \cdot (\kappa_V \nabla P) = -2\lambda_V(\delta P - \delta\pi). \quad [7]$$

322 The permeation coefficient λ_V can, in principle, differ in the 323
 323 cleft compared its value in the lumen. For the sake of sim- 324
 324 plicity, we use the same value. From here on, and for similar 325
 325 reasons as for ion flux, the time derivative of the thickness can 326
 326 be neglected based on the time scale we consider for lumen 327
 327 expansion (see SI Appendix (2)). 328

329 **Strategy to solve the equations.** The complete set of equations 330
 330 that we solve is provided in SI Appendix (4). To solve the 331
 331 equations, we assume that the parameters of the cytosol and 332
 332 of the external media are constant and homogeneous. We also 333
 333 assume that the variation in ion concentration $\delta\rho$, is small 334
 334 compared to the concentrations themselves. 335

335 Separating the time scales between lumen dynamics (minutes 336
 336 to hours) and the equilibrium of fluxes in the cleft (sub seconds) 337
 337 simplifies the problem. Cleft equations (3,5,7) are solved in 338
 338 the quasistatic regime. The ion density in the cleft readily 339
 339 stems from Eq. (5). We then use it as a source term in Eq. (7). 340
 340 The solution of Eq. (7) leads to the value of $j_i^{l \rightarrow c}$, which can 341
 341 in turn can be used in Eq. (4) and Eq. (6). We thus reduce 342
 342 the problem to three coupled equations that we formally solve 343
 343 using Mathematica. SI Appendix Table S1 summarizes the 344
 344 various parameters of the problem and we give their ranges in 345
 345 adimensional and real values in SI Appendix (1). 346

347 Existence of Steady states

348 At steady state, the dynamical equations above simplify as 349
 349 follows. We name R_s, r_s and θ_s the lumen dimensions at 350
 350 steady state. 351

352 **Steady state mechanical balance.** The Young-Dupr e relation 353
 353 takes the simple form 354

$$355 \cos \theta_s = \frac{\bar{\sigma}}{\sigma_0} = 1 - \frac{E}{\sigma_0}. \quad [8]$$

357 In this expression σ_0 is the steady state tension, and θ_s is thus 358
 358 a constant determined by the tension and adhesion energy at 359
 359 steady state. We take it equal to $\frac{\pi}{6}$ following experimental 360
 360 observations (10). 361

362 **Steady state ion conservation.** Assuming azimuthal symmetry, 363
 363 the ion conservation in the **cleft** (eq.5) can be linearized at 364
 364 the first order in polar coordinates as: 365

$$366 -\xi_i^2 \frac{1}{r} \frac{\partial}{\partial r} \left(r \frac{\partial}{\partial r} \delta\rho(r) \right) + \delta\rho(r) = \delta\rho_i. \quad [9]$$

367 With the continuity equations at the cleft edges being: 368

$$369 \begin{cases} \delta\rho(r)|_{r=r_l} & = \delta\rho \text{ at the lumen-cleft edge} \\ \delta\rho(r)|_{r=L} & = \delta\rho_{ext} \text{ at the cleft-external medium edge} \end{cases}$$

373 $\delta\rho_i = \frac{\rho_{cell}j_i}{2k_B T \lambda_i}$ acts as a source term and compares pumping
 374 activity to passive ion transport. It corresponds to the ion
 375 concentration which would be observed in the cleft if there was
 376 a simple balance between pumps and channels. It characterizes
 377 the "pumping efficiency". Note that since $\delta\rho_i$ is a constant,
 378 Eq. (9) admits a simple although cumbersome solution in terms
 379 of modified Bessel functions, which we give in SI Appendix
 380 (3).

381 $\xi_i = \sqrt{\frac{D\rho_{cell}}{2k_B T \lambda_i}}$ is the typical length over which the ion
 382 concentration is screened from the edge effects to reach the
 383 constant value set by $\delta\rho_i$. When $L - r_l \gg \xi_i$ (i.e long cleft and
 384 small lumen), the leaks at both edges of the cleft are decoupled
 385 from the central part of the cleft the ion density of which only
 386 depends on $\delta\rho_i$. Additionally, if $\delta\rho_i > \delta\rho$ then, the ion flux
 387 $j_i^{l \rightarrow c}$ corresponds to an ion source for the lumen. When the
 388 lumen is large (i.e $L - r_l \sim \xi_i$), the leaks at both edges of the
 389 cleft couple to the lumen to create a paracellular concentration
 390 gradient. If $\delta\rho > \delta\rho_{ext}$ the ion flux $j_i^{l \rightarrow c}$ corresponds to a
 391 sink for the lumen which takes the simple expression, in the
 392 limit ($L - r_l \ll \xi_i$):

$$393 \quad j_i^{l \rightarrow c} \approx \frac{De(\rho_{lum}^i - \rho_{ext}^i)}{L - r_l}. \quad [10]$$

394 In the **lumen** the ion conservation (4) then simplifies as:

$$395 \quad 2R_s(1 - \cos \theta_s)(\delta\rho - \delta\rho_i) = \xi_i^2 \left(\frac{\partial}{\partial r} \delta\rho \right) \Big|_{r=r_l}. \quad [11]$$

396 where $\left(\frac{\partial}{\partial r} \delta\rho \right) \Big|_{r=r_l}$ takes the expression derived from the expres-
 397 sion $\delta\rho$ derived in SI Appendix (3). For the sake of simplicity
 398 we assume here that the pump activity in the cleft equals that
 399 of the lumen.

400 **Steady state volume conservation**. In the **cleft** Eq. 7 can be
 401 simplified in a similar way and writes:

$$402 \quad -\xi_V^2 \frac{1}{r} \frac{\partial}{\partial r} \left(r \frac{\partial}{\partial r} \delta P(r) \right) + \delta P(r) = \delta\pi. \quad [12]$$

403 with the continuity of the hydrostatic pressure at both edges
 404 imposing :

$$405 \quad \begin{cases} \delta P(r) \Big|_{r=r_l} = \delta P_{lum} & \text{at the lumen-cleft edge} \\ \delta P(r) \Big|_{r=L} = \delta P_{ext} & \text{at the cleft-external medium edge} \end{cases}$$

406 The solution is also tractable analytically (see SI Appendix
 407 (3)).

408 $\delta\pi = 2k_B T \delta\rho$ is the source term from osmotic origin.
 409 $\xi_V = \sqrt{\frac{\kappa}{2\lambda_V}}$ is another screening length, comparing the ef-
 410 ficiency of the hydrodynamic leak to aquaporin transport.
 411 When $L - r_l \gg \xi_V$, the lumen and the external medium are
 412 decoupled. In particular when $L - r_l \gg \xi_V$ and ξ_i then the
 413 hydrostatic pressure in the cleft away from the edges is entirely
 414 imposed by the pumps and equals $2k_B T \delta\rho_i$.

415 Whenever the cleft length is longer than both screening lengths,
 416 it acts as a volume source for the lumen. In the opposite case
 417 (i.e $L - r_l \sim \xi_V$) provided that $P_{ext} < P_{lum}$, the cleft
 418 contributes to a volume leak out of the lumen that simplifies
 419 to

$$420 \quad j_v^{l \rightarrow c} \approx \frac{\lambda_v(P_{lum} - P_{ext})}{L - r_l}. \quad [13]$$

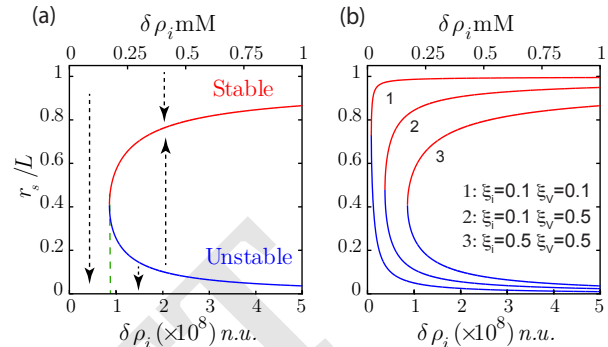
421 when ($L - r_l \ll \xi_V$).

422 In the **lumen**, Eq 6 simplifies as

$$423 \quad 2R_s(1 - \cos \theta_s) \left(\frac{2\sigma_0}{R_s} - 2k_B T \delta\rho \right) = \xi_V^2 \left(\frac{\partial}{\partial r} \delta P \right) \Big|_{r=r_l}. \quad [14]$$

424 The right hand term is derived from Eq. 12 (see SI Appendix
 425 (3)) and taking its value for r_l .

426 This rescaling of the equations reveals that the relevant
 427 parameters controlling the lumen are $\delta\rho_i$, ξ_i , ξ_V and θ_s . They
 428 compare the strength of the various fluxes. They arise from a
 429 combination of the more natural parameters ρ_{cell} , κ_V , D , j_i ,
 430 λ_i , λ_V and θ_s , introduced in the first sections to characterize
 431 the fluxes themselves. For all parameter values, the solutions



432 **Fig. 3.** a: The steady state size of the lumen as a function of pumping efficiency
 433 displays an unstable and a stable branch represented in blue and red respectively
 434 ($\xi_V = \xi_i = 0.5$). The dashed arrows represent the direction of variation of lumen
 435 radius for any deviation from its steady state value. There is no stable state lumen
 436 at low enough pumping efficiency $\delta\rho_i$. Any lumen of any size would shrink off. Above
 437 a critical $\delta\rho_i$, any small lumen above the unstable branch will grow to finally reach
 438 a larger steady lumen size. b: variation of the steady lumen size as a function of
 439 lumen efficiency for different screening lengths ξ_V and ξ_i .

440 for the steady state lumen radius are qualitatively similar to
 441 the one described in Fig.3. For a given leak (characterized
 442 by the values of ξ_i and ξ_V) there exist a critical value of the
 443 ion pumping activity (characterized by $\delta\rho_i$), below which no
 444 lumen can exist.

445 Low enough pumping activity cannot compensate the leaks.
 446 Independently of its original volume, the lumen shrinks
 447 and disappears. When the pump activity is higher, the
 448 solution displays two branches. The lower branch is unstable
 449 and theoretically corresponds to the creation of a lumen
 450 through the nucleation of a small sized cavity inside the cleft.
 451 The instability of this solution can be checked directly on
 452 dynamical equations, but it can also be understood with the
 453 following argument.

454 Steady state lumens described by lower branches are small
 455 ($L - r_s > \xi_i$ and ξ_V). A small increase in lumen size leads to
 456 a rise in the incoming fluxes, which is due to an increase in
 457 lumen surface. However, in this limit the paracellular fluxes
 458 are hardly affected by the change in size due to the screening
 459 of the leak. Moreover, the osmotic pressure increases, whereas
 460 the Laplace term decreases due to tension. Here, the chemical
 461 potential balance fails, which leads to further growth. All
 462 contributions lead to further volume increase. Although
 463 predicted by the model, this solution is likely to be obscured
 464 in reality by the more complex biological and molecular
 465 organization needed to start lumen formation.

466 The upper branches correspond to stable solutions for larger

497 lumens ($L - r_s \sim \xi_i$ and ξ_V). If the lumen grows, the
 498 incoming fluxes also grow. However Eq. (10) and Eq. (13)
 499 show that in this limit, the paracellular fluxes diverge as
 500 the lumen size approaches the size of the junction. This
 501 non linear dependence of the paracellular leak in this limit,
 502 enables the a stability of the state. The sensitivity to the
 503 edge distance is thus governed by the screening lengths ξ_i
 504 and ξ_V . Fig.3b shows that small screening lengths (curve
 505 1) result in stable lumens spanning practically the whole
 506 cell-cell contact for all pumping activities. Conversely, large
 507 screening lengths (curve 3) confine lumens to smaller sizes
 508 above a critical pumping activity. One could thus speculate
 509 that the ability of lumens from adjacent cell pairs to merge
 510 is determined by their ability to reach the cell edges, and is
 511 hence controlled by the leak properties of the paracellular cleft.

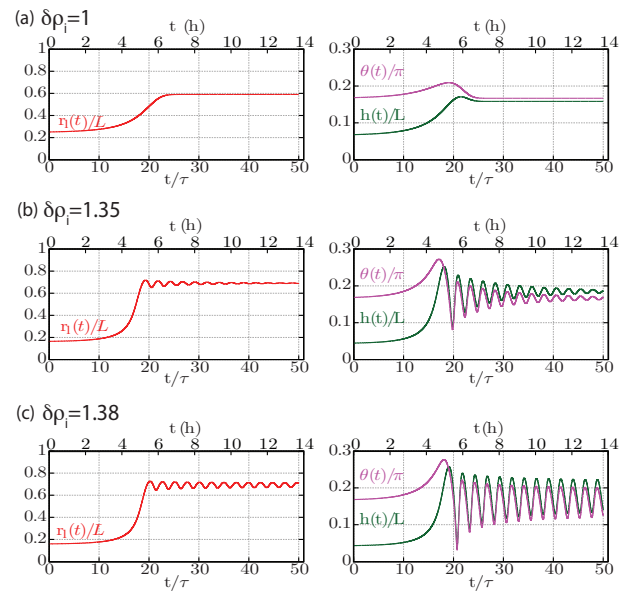
512 Lumen dynamics

513
 514
 515 The balance between different fluxes not only determines the
 516 steady states of the lumen, but also affects lumen dynamics.
 517 Fig.1c-d shows that lumen growth can be either monotonous
 518 or pulsatile, depending on pumping efficiency. Our model
 519 suggests that changing the balance between leaks and ion
 520 secretion can induce a transition between both behaviors. The
 521 periodicity of the experimental pulsations are of the order
 522 of tens of minutes. Consequently, we assume a quasi-static
 523 mechanical equilibrium in the cleft. We solve equations 4-2
 524 as described in SI Appendix (5). The time dependent variables
 525 of the problem are the radius of curvature $R(t)$, the contact
 526 angle $\theta(t)$ and the difference of ion concentration in the lumen
 527 with respect to the cytosol $\delta\rho(t)$. The lumen shape and volumes
 528 can be deduced by simple geometric relations. The cortical
 529 tension σ must account for the lumen expansion. In situations
 530 where the change per unit time of relative cortex area becomes
 531 "large", then one must account for a viscous term as a dominant
 532 contribution to the periluminal stress. This results in an a real
 533 strain rate dependent effective tension. A characteristic time
 534 τ_c delineates these two behaviors. In an active gel description
 535 of the cortex the effective tension can be written as (19):

$$536 \sigma(t) = \sigma_0 \left[1 + \tau_c \left(\frac{dR(t)}{R(t)} + \frac{d\theta(t)}{2(1 - \cos\theta(t))} \right) \right]. \quad [15]$$

537
 538 where the quantity $\left(\frac{dR(t)}{R(t)} + \frac{d\theta(t)}{2(1 - \cos\theta(t))} \right)$ is a measure of
 539 the deformation rate, which we take to be equal to the relative
 540 time variation of the lumen area. The static value of the
 541 tension σ_0 is set by imposing a value of $\frac{\pi}{6}$ to θ_s . All other
 542 coefficients are assumed constant. The dynamical equations
 543 are expressed in SI Appendix (4).

544 To exemplify the type of behavior predicted by the model,
 545 we fixed the screening length to $\xi_V = 0.49$, and $\xi_i = 0.50$ and
 546 we solved the dynamical equation at different values of the
 547 pumping efficiency $\delta\rho_i$. We set the initial conditions for the
 548 lumen height $R(t)$, $\theta(t)$, $\delta\rho(t)$, $\sigma(t)$ just above the unstable
 549 branch of the lumen steady state (SI Appendix Table 2). In
 550 our model this would correspond to a lumen growing from its
 551 nucleation size. However the final behavior of the dynamics
 552 does not depend on initial conditions. Fig. 4 shows that at
 553 lower pumping efficiency, the steady state of the lumen is
 554 reached monotonically with a mild overshoot in the contact
 555 angle and lumen height. At larger pumping efficiency, the



556
 557
 558
 559
 560
 561
 562
 563
 564
 565
 566
 567
 568
 569
 570
 571
 572
 573
 574
 575
 576
 577
 578
 579
 580
 581
 582
 583
 584
 585
 586
 587
 588
 589
 590
 591
 592
 593
 594
 595
 596
 597
 598
 599
 600
 601
 602
 603
 604
 605
 606
 607
 608
 609
 610
 611
 612
 613
 614
 615
 616
 617
 618
 619
 620

Fig. 4. Dynamical behavior of the normalized lumen height $h(t)/L$, junctional extension $r_l(t)/L$ and angle $\theta(t)/\pi$ are shown as a function of normalized time t/τ (lower abscissa) and time in hours (upper abscissa), where $\tau = 2 \times 10^{-8}$ n.u. is the cortex time (assumed 1000 s). Changing pump efficiency $\delta\rho_i$ shows three different characteristic behavior- (a) Overdamped evolution towards steady state at $\delta\rho_i = 1.0 \times 10^8$ n.u. (b) Underdamped evolution towards steady state at $\delta\rho_i = 1.35 \times 10^8$ n.u. and (c) Sustained oscillations $\delta\rho_i = 1.38 \times 10^8$ n.u.. The numerics has been obtained for values of $\xi_V = 0.49$, $\xi_i = 0.50$, $\Lambda_v = 1$ n.u., $\Lambda = \Lambda_i k_B T \tau / \rho_{cell} L = 1.1 \times 10^8$ n.u., $\sigma_0 = 10^7$ n.u., $\delta\rho_{ext} = -2 \times 10^6$ n.u., and $\rho_{cell} = 10^9$ n.u..

steady state is reached after damped oscillations. At large
 pumping efficiency the oscillations are sustained. An ani-
 mation of lumen dynamics in each scenario can be found in
 Supplementary Videos 1-3. The existence of the oscillations
 originates from the nonlinearity of the equations, in particular
 from the divergence of the leak close to the contact edge. How-
 ever we could not trace one specific parameter alone that was
 primarily responsible for setting the behavior. In SI Appendix
 (3) we derive an analytical solution in the transition regime in
 the limit for large enough lumens ($L - r_l \ll \xi_i$, $L - r_l \ll \xi_V$)
 and for small deviations from steady state values of the vari-
 ables. In the simplified equations, terms analogous to inertia,
 friction and force could be introduced (respectively a,b and c
 in SI Appendix (3)); their expressions intricately involve all
 model parameters. However, the cross over limits between
 the different dynamic behaviors is set by the parameter τ_c ,
 which reflects the dependence of cortical tension on strain rate.
 Using a constant tension, our numerical solutions do not show
 any oscillatory behavior within the physiological range of the
 parameters we explored.

We then calculated the time variation of the lumen concen-
 tration (Fig. 5). In all cases the concentration of the lumen
 decreases as the lumen grows. It oscillates in phase opposition
 with the lumen radius in the oscillatory regime. Note however
 that the total amount of ions $\delta\rho \times V$ increases with the lumen
 size. The cortical tension varies during the formation of the
 lumen, increases during the growth phase, and equals σ_0 for
 the steady states. It oscillates in phase with the lumen radius
 in the oscillatory case. The inner hydrostatic pressure of the
 lumen calculated from Laplace's law decreases as the lumen

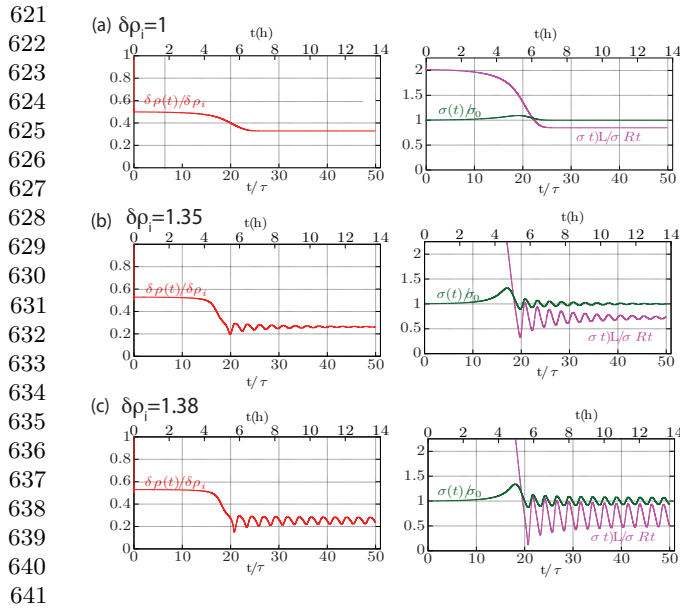


Fig. 5. Dynamical behavior of the normalized lumen ion-density $\delta\rho(t)/\delta\rho_i$, lumen tension $\sigma(t)/\sigma_0$, and hydrostatic pressure $\frac{\sigma(t)/R(t)}{\sigma_0/L}$ for different pump efficiency $\delta\rho_i$ are shown as a function of time t/τ (lower abscissa) and time in hours (upper abscissa), where $\tau = 2 \times 10^{-8}$ n.u. is the cortex time (assumed 1000 s). Changing pump activity shows three different characteristic behavior- (a) Monotonous overdamped evolution towards steady state at $\delta\rho_i = 1.0 \times 10^8$ n.u. (b) Underdamped evolution towards steady state at $\delta\rho_i = 1.35 \times 10^8$ n.u. and (c) Sustained oscillations $\delta\rho_i = 1.38 \times 10^8$ n.u.. All parameters used for obtaining the numerics are the same as those mentioned in Fig. 4.

grows and oscillates in phase opposition with the lumen radius in the oscillatory regime. Our model thus predicts that as the lumen grows the effective periluminal tension grows due to an induced viscous stress. It is qualitatively different from a mechanosensitive feed back that would lead to an active reinforcement of the cortex. Additionally, as the lumen grows the inner pressure decreases. This is the opposite of the "Starling's law" like interpretation of a lumen growing under an increasing inner pressure, leading to a final contraction that expels the inner fluid. Whereas this later scenario is possible in fully sealed lumen, our model demonstrates that the same dynamical behavior can also be recapitulated in leaking lumens.

Discussion

The situation of a cavity with constant ion secretion and a fixed cortical tension is intrinsically unstable. A steady state can only be achieved upon three non exclusive conditions: size or time dependent cortical tension, size or time dependent ion secretion, and/or leaks. The two first conditions are likely to involve specific biological feedback. The incidence of leaks is far less intuitive to understand. The model we propose quantitatively explores the effect of paracellular leakage in the case of intercellular lumen formation. We account for the specific dependence of the leak

on the dimensions of the paracellular cleft, and we show that, in the case of a bicellular lumens, the leak can play a critical role in controlling lumen size, dynamics and composition. The model provides a good qualitative agreement with the experimental phenotypes of canaliculi.

An important prediction of the model is the existence of screening lengths ξ_s, ξ_v . The screening lengths compare longitudinal fluxes along the cleft that are mediated by osmotic potential differences and hydrostatic pressure, to the transmembrane fluxes that occur orthogonal to the cleft and are mediated by channels. When transmembrane transport outweighs paracellular transport, the screening lengths are small. Curve 1 on Figure 3 shows that in this case the lumen can grow close to the edges ($r_s \sim L$). In contrast, in the case of a large screening length (curve 3) the lumen hardly reaches the cell edge independently of pump activity. The lumen composition, i.e its ion concentration, is also affected by the screening length values. Figure 6a shows that when the distance of the lumen to the cell edge is larger than the screening length the luminal ion concentration is of the same order as $\delta\rho_i$; the equilibrium value for a close lumen. As the lumen grows towards the contact edges, paracellular leaks increase, leading to a decrease in ion density, and hence, of the osmotic pressure as well as hydrostatic pressure. However, Figure 6b, shows that the osmotic pressure decreases considerably less than the hydrostatic pressure. This results in lumens with a much higher ion concentration than what is needed to balance Laplace pressure, should the lumen be closed. Our simplifying assumptions minimize the

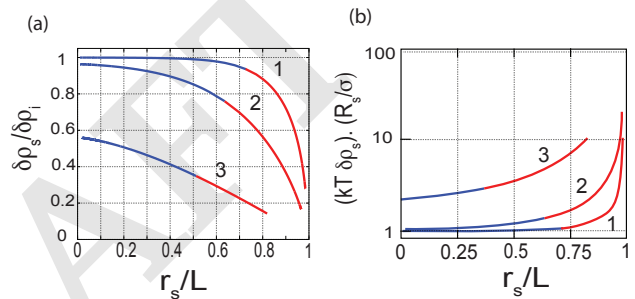


Fig. 6. a: Comparison of steady state ion density in the lumens of various sizes with the expected concentration ($\delta\rho_i$). $\xi_i = 0.1$ for all curves. For curves (1) $\xi_v = 0.1$, Curves (2) $\xi_v = 0.2$, Curves (3) $\xi_v = 0.5$. b: comparison of the lumen osmotic pressure to the Laplace pressure as a function of lumen size for different screening lengths.

specific biological details that have yet to be accounted for to perform a quantitative comparison with experimental data. In particular, tight junctions act as diffusive barriers for different classes of ions across claudin pores(20, 21). For the sake of simplicity we account for their activity as a steady factor included in the hydrodynamic resistance of the paracellular cleft. As the tight junctions mature their contribution to the paracellular leak might become dominant over the simple evaluation, which is based on a hydrodynamic process. In particular, ion flux selectivity, which enhanced junction stability and mechanosensitivity of tight junctions, may then play a role in the homeostasis of lumens.

We also show that a time dependent cortical tension is necessary to create an oscillatory behavior. In our model, the origin of cortical tension reinforcement stems from cortex dynamics. As previously mentioned, mechanosensitive mechanisms might reinforce cortex contractility by increasing the actomyosin activity in a stress dependent manner. However, as shown in Figure. 5 the hydrostatic pressure decreases as the lumen grows, and it is not clear where the mechanosensing reinforcement of the cortex would come from within the

745 frame of this model. Although lipid trafficking by endo and
746 exocytosis (1) is important for lumen growth, our model
747 indirectly accounts for it as a non limiting factor of the lumen
748 expansion. Assuming a non limiting rate supply of lipids by
749 vesicular transport, their contribution to cortical tension and
750 thus lumen morphology is negligible. We also do not account
751 for vesicular export of bile in cholestasis cases corresponding
752 to a liver specific problem that would reduce the generality of
753 our description. We indeed propose that the leak dependent
754 growth of lumens can be extended to understand, at the
755 tissue scale, the direction of growth of the cavities. In the case
756 described here, the lumen edge can only asymptotically reach
757 the contact edge due to the divergence of the paracellular leak
758 when r_l approaches L . Consider now a single lumen with equal
759 pumping efficiency but embedded in a group of cells rather
760 than a cell doublet. One can qualitatively assume that the
761 resistance to paracellular flux will depend on the total length
762 of paracellular cleft between the lumen edge and the external
763 medium. L would then be much larger than the actual size
764 of a single cell-cell contact. In such a case, our model would
765 predict that the lumen radius can extend further than a single
766 cell length and consequently could bridge with other adjacent
767 lumens. Maintaining the same assumptions, the problem
768 of lumen now depends on the structure of the tissue. This
769 more intricate study lies beyond the scope of this work un-
770 derstood as a foundation more elaborate analyses in the future.

771

772

773

774

775

776

777

778

779

780

781

782

783

784

785

786

787

788

789

790

791

792

793

794

795

796

797

798

799

800

801

802

803

804

805

806

1. Sigurbjörnsdóttir S, Mathew R, Leptin M (2014) Molecular mechanisms of de novo lumen formation. *Nature reviews. Molecular cell biology* 15(10):665–76.
2. Sperber I (1959) Secretion of organic anions in the formation of urine and bile. *Pharmacol Rev* 11(1):109–34.

3. Boyer JL (2013) Bile formation and secretion. *Compr Physiol* 3(3):1035–78.
4. Bryant DM, Mostov KE (2008) From cells to organs: building polarized tissue. *Nat Rev Mol Cell Biol* 9(11):887–901.
5. Andrew DJ, Ewald AJ (2010) Morphogenesis of epithelial tubes: Insights into tube formation, elongation, and elaboration. *Dev Biol* 341(1):34–55.
6. Roignot J, Peng X, Mostov K (2013) Polarity in mammalian epithelial morphogenesis. *Cold Spring Harb Perspect Biol* 5(2).
7. Ruiz-Herrero T, Alessandri K, Gurchenkov BV, Nassoy P, Mahadevan L (2017) Organ size control via hydraulically gated oscillations. *Development* 144(23):4422–4427.
8. Gupta K, et al. (2017) Actomyosin contractility drives bile regurgitation as an early response during obstructive cholestasis. *Journal of Hepatology*.
9. Lipowsky R, Sackmann E (1995) *Handbook of biological physics, Structure and Dynamics of Membranes*. (Elsevier) Vol. 1.
10. Li Q, et al. (2016) Extracellular matrix scaffolding guides lumen elongation by inducing anisotropic intercellular mechanical tension. *Nat Cell Biol* 18(3):311–8.
11. Watanabe S, et al. (1988) Bile canalicular contraction in the isolated hepatocyte doublet is related to an increase in cytosolic free calcium ion concentration. *Liver International* 8(3):178–183.
12. Clair C, et al. (2001) Investigation of the roles of ca^{2+} and $insp3$ diffusion in the coordination of ca^{2+} signals between connected hepatocytes. *Journal of cell science* 114(11):1999–2007.
13. Dong B, et al. (2009) Tube formation by complex cellular processes in Ciona intestinalis notochord. *Developmental Biology* 330(2):237–249.
14. Dong B, Hannezo E, Hayashi S (2014) Balance between apical membrane growth and luminal matrix resistance determines epithelial tubule shape. *Cell Reports* 7(4):941–950.
15. Schlüter MA, Margolis B (2009) Apical lumen formation in renal epithelia. *Journal of the American Society of Nephrology* 20(7):1444–1452.
16. Fütterer C, Colombo C, Jülicher F, Ott A (2003) Morphogenetic oscillations during symmetry breaking of regenerating hydra vulgaris cells. *Europhys. Lett.* 64(1):137–143.
17. Turlier H, Audoly B, Prost J, Joanny JF (2014) Furrow Constriction in Animal Cell Cytokinesis. *Biophysical Journal* 106(1):114–123.
18. Sackmann E, Smith AS (2014) Physics of cell adhesion: some lessons from cell-mimetic systems. *Soft Matter* 10(11):1644–59.
19. Kruse K, Joanny JF, Jülicher F, Prost J, Sekimoto K (2005) Generic theory of active polar gels: a paradigm for cytoskeletal dynamics. *Eur Phys J E Soft Matter* 16(1):5–16.
20. Adamson RH, et al. (2004) Oncotic pressures opposing filtration across non-fenestrated rat microvessels. *The Journal of Physiology* 557(3):889–907.
21. Cattaneo I, et al. (2011) Shear stress reverses dome formation in confluent renal tubular cells. *Cellular Physiology and Biochemistry* 28(4):673–682.

807
808
809
810
811
812
813
814
815
816
817
818
819
820
821
822
823
824
825
826
827
828
829
830
831
832
833
834
835
836
837
838
839
840
841
842
843
844
845
846
847
848
849
850
851
852
853
854
855
856
857
858
859
860
861
862
863
864
865
866
867
868